

Online learning of eddy-viscosity and backscattering closures for geophysical turbulence using ensemble Kalman inversion

Yifei Guan^{1,2,†}, Pedram Hassanzadeh^{1,‡}, Tapio Schneider³, Oliver Dunbar³, Daniel Zhengyu Huang^{3,4}, Jinlong Wu⁵, and Ignacio Lopez-Gomez^{3,6}

¹University of Chicago, Chicago, IL 60637, USA

²Union College, Schenectady, NY 12308, USA

³California Institute of Technology, Pasadena, CA 91125, USA

⁴Peking University, Beijing, 100871, China

⁵University of Wisconsin–Madison, Madison, WI 53706, USA

⁶Google Research, Mountain View, CA 94043, USA

(Received xx; revised xx; accepted xx)

Different approaches to using data-driven methods for subgrid-scale closure modeling have emerged recently. Most of these approaches are data-hungry, and lack interpretability and out-of-distribution generalizability. Here, we use online learning to address parametric uncertainty of well-known physics-based large-eddy simulation (LES) closures: the Smagorinsky (Smag) and Leith eddy-viscosity models (1 free parameter) and the Jansen-Held (JH) backscattering model (2 free parameters). For 8 cases of 2D geophysical turbulence, optimal parameters are estimated, using ensemble Kalman inversion (EKI), such that for each case, the LES' energy spectrum matches that of direct numerical simulation (DNS). Only a small training dataset is needed to calculate the DNS spectra (i.e., the approach is data-efficient). We find the optimized parameter(s) of each closure to be constant across broad flow regimes that differ in dominant length scales, eddy/jet structures, and dynamics, suggesting that these closures are generalizable. In a-posteriori tests based on the enstrophy spectra and probability density functions (PDFs) of vorticity, LES with optimized closures outperform the baselines (LES with standard Smag, dynamic Smag or Leith), particularly at the tails of the PDFs (extreme events). In a-priori tests, the optimized JH significantly outperforms the baselines and optimized Smag and Leith in terms of interscale enstrophy and energy transfers (still, optimized Smag noticeably outperforms standard Smag). The results show the promise of combining advances in physics-based modeling (e.g., JH) and data-driven modeling (e.g., online learning with EKI) to develop data-efficient frameworks for accurate, interpretable, and generalizable closures.

Key words: Large-eddy simulation, Data-driven closure modeling, Geophysical turbulence

† Email address for correspondence: guany@union.edu

‡ Email address for correspondence: pedramh@uchicago.edu

1. Introduction

Recent advances in data-driven methods offer new avenues to develop better subgrid-scale (SGS) closures (parameterizations), which are essential, for example, for large-eddy simulations (LES) of geophysical turbulence in critical applications such as climate modeling (e.g., Schneider *et al.* 2023; Sanderse *et al.* 2024; Lai *et al.* 2024; Eyring *et al.* 2024; Bracco *et al.* 2024). Most studies have focused on *offline* (supervised) learning, in which a closure is developed, for instance, by training neural networks (NNs) or using equation-discovery algorithms to match the true and parameterized SGS fluxes (e.g., Maulik *et al.* 2019; Beck *et al.* 2019; Zanna & Bolton 2020; Guan *et al.* 2022; Jakhar *et al.* 2024). The trained/discovered closure, once validated *a-priori*, is coupled to a low-resolution solver (e.g., a climate model) for *a-posteriori* tests. While examples of stable and accurate SGS modeling using *offline* learning with NNs have emerged recently (e.g., Guan *et al.* 2023; Srinivasan *et al.* 2024; Ross *et al.* 2023; Yuval & O’Gorman 2023), this approach has major drawbacks: 1) training NNs require many samples of the “true” SGS fluxes, 2) these closures are largely uninterpretable, and 3) they do not generalize out-of-distribution (extrapolate) to other flows (e.g., higher Reynolds numbers, Re); see, e.g., Rasp *et al.* (2018); Subel *et al.* (2023); Beucler *et al.* (2024). Item (1) is a major practical challenge as it requires long, expensive, high-resolution simulations (e.g., direct numerical simulations, DNS). Also, estimating the true SGS fluxes from such data is difficult (Jakhar *et al.* 2024; Sun *et al.* 2023).

An alternative is *online* (aka end-to-end) learning: the closure is developed while it is coupled to the low-resolution solver, with the objective of matching certain statistics of the “true” flow (e.g., from high-resolution simulations or even observations). If the existing closures have “structural uncertainties”, then NNs can be used to learn either the entire closure from data (e.g. Kennedy & O’Hagan 2002) or corrections to physics-based closures (e.g. Wu *et al.* 2024). However, minimizing the loss function of this approach can be practically challenging (see below); that said, promising results with NNs trained using ensemble Kalman inversion (EKI) (Pahlavan *et al.* 2024), multi-agent reinforcement learning (Novati *et al.* 2021; Mojgani *et al.* 2023), and differentiable modeling (Sirignano *et al.* 2020; Frezat *et al.* 2022; List *et al.* 2022; Shankar *et al.* 2023) have started to appear. While this approach addresses item (1), interpretability and generalization ((2)-(3)) remain major challenges.

One avenue for addressing (1)-(3) is to develop closures with the appropriate structure using physical arguments (and when needed, equation-discovery techniques), and use *online* learning to estimate the unknown parameters (i.e., addressing “parametric uncertainty”); see Schneider *et al.* (2021) for further discussions and Schneider *et al.* (2023, 2024), Lopez-Gomez *et al.* (2022), Zhang *et al.* (2022), and Martinez *et al.* (2024) for recent examples of success with this approach. The major question about this approach is whether one is simply calibrating/tuning a closure for limited metrics, such that the calibrated closure does not work well for other metrics. Furthermore, generalization (3) requires the estimated parameters to be universal constants (or at least nearly invariant within the flow regimes of interest). These questions, even for canonical test cases, remain to be fully investigated.

In this paper, we aim to answer these questions for several setups of 2D turbulence, a canonical model for many geophysical flows. We estimate the parameters of two classical eddy-viscosity closures (Smagorinsky and Leith) and a new backscattering closure (Jansen & Held 2014) *online* using EKI and by matching the energy spectrum of LES with that of a short DNS (truth). The LES with EKI-optimized parameters,

Case	1.1	1.2	1.3	1.4	2	3.1	3.2	3.3
Re	20000	20000	100000	300000	20000	20000	100000	300000
k_f	4	4	4	4	4	25	25	25
β	0	0	0	0	20	0	0	0
N_{DNS}	1024	1024	4096	4096	1024	1024	4096	4096
N_{LES}	32	64	256	256	64	256	256	256
$C_{\text{S}}^{\text{EKI}}$	0.12	0.12	0.11	0.12	0.10	0.12	0.12	0.10
$C_{\text{L}}^{\text{EKI}}$	0.23	0.25	0.26	0.24	0.21	0.24	0.23	0.21
$C_{\text{JHS}}^{\text{EKI}}, C_{\text{B}}^{\text{EKI}}$	0.23, 0.96	0.22, 0.95	0.21, 0.95	0.21, 0.95	0.20, 0.94	0.22, 0.94	0.23, 0.95	0.21, 0.96
$C_{\text{JHL}}, C_{\text{B}}^{\text{EKI}}$	0.31, 0.94	0.30, 0.96	0.31, 0.95	0.30, 0.96	0.28, 0.95	0.30, 0.95	0.30, 0.96	0.28, 0.96

Table 1: Top: Physical and numerical parameters of the 8 cases. Bottom: EKI-optimized parameters (uncertainties are shown in Supplementary Material Table 1).

which are found to be constants across cases, are then examined in terms of enstrophy spectra, interscale transfers, and probability density functions (PDFs) of vorticity, especially at the tails (extreme events).

2. Data and Methods

2.1. DNS and LES of 2D turbulence

We use 8 setups of forced 2D β -plane turbulence. The dimensionless governing equations in the vorticity (ω) and streamfunction (ψ) formulation in a doubly periodic square domain of length $L = 2\pi$ are

$$\frac{\partial \omega}{\partial t} + \mathcal{N}(\omega, \psi) = \frac{1}{Re} \nabla^2 \omega - f - r\omega + \beta \frac{\partial \psi}{\partial x}, \quad \nabla^2 \psi = -\omega. \quad (2.1)$$

Here, \mathcal{N} is the Jacobian, $f(x, y) = k_f[\cos(k_f x) + \cos(k_f y)]$ is a deterministic forcing, and $r = 0.1$ is the linear drag coefficient (e.g., representing surface friction); β is the gradient of the Coriolis parameter. We study 8 cases, in which Re , forcing wavenumber (k_f), and β have been varied (Table 1), creating a variety of flows that differ in dominant length scales and energy/enstrophy cascade regimes (Fig. 1). For DNS, which is treated as the truth, Eqs. (2.1) are solved at high spatial-temporal resolutions ($N_{\text{DNS}}^2 \times \Delta t_{\text{DNS}}$) using a Fourier pseudo-spectral solver (see Guan *et al.* 2022). The LES equations are derived by applying a low-pass filter (e.g., sharp cut-off), denoted by $\overline{(\cdot)}$, to (2.1):

$$\frac{\partial \overline{\omega}}{\partial t} + \mathcal{N}(\overline{\omega}, \overline{\psi}) = \frac{1}{Re} \nabla^2 \overline{\omega} - \overline{f} - r\overline{\omega} + \beta \frac{\partial \overline{\psi}}{\partial x} - \underbrace{\left[\overline{\mathcal{N}(\omega, \psi)} - \mathcal{N}(\overline{\omega}, \overline{\psi}) \right]}_{\Pi^{\text{SGS}} = \nabla \times (\nabla \cdot \tau^{\text{SGS}})}, \quad \nabla^2 \overline{\psi} = -\overline{\omega}. \quad (2.2)$$

Solving these equations needs much coarser resolutions ($N_{\text{LES}}^2 \times 10\Delta t_{\text{DNS}}$), where $N_{\text{DNS}}/N_{\text{LES}}$ is between 4 and 32 (Table 1). The SGS term, Π^{SGS} or τ^{SGS} , requires a closure.

2.1.1. Physics-based closures with parametric uncertainty

Eddy-viscosity closures are “functional” models that assume the net effect of the SGS term is dissipation of the resolved scales: $\tau^{\text{SGS}} = -2\nu_e \bar{S}$, where \bar{S} is the rate of strain

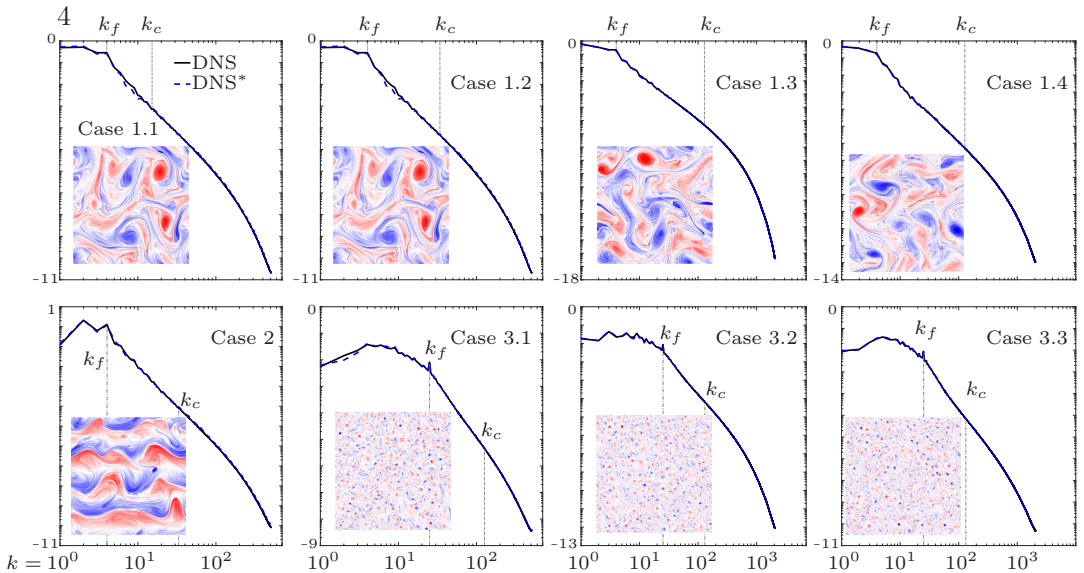


Figure 1: The TKE spectra ($\log_{10}(\hat{E}(k))$) and examples of ω for each case. The k_f and k_c are marked. The black (blue) lines show DNS spectra averaged over all 100 (first 5) snapshots in the training set. With a sharp-spectral cut-off filter, the FDNS spectrum, which is used as the target in Eq. (2.4), overlaps with the DNS spectrum over $k = [0, k_c]$.

of the resolved flow, and $\nu_e(x, y, t)$ is the eddy-viscosity (Sagaut 2006). For 2D turbulence, the Smagorinsky (1963) model (Smag: $\nu_e = (C_S \Delta)^2 \langle \mathcal{S}^2 \rangle^{1/2}$, $\Delta = L/N_{LES}$) and the Leith (1996) model (Leith: $\nu_e = (C_L \Delta)^3 \langle (\nabla \bar{\omega})^2 \rangle^{1/2}$) are often used in practice, with C_S and C_L being parameters to be determined ($\langle \cdot \rangle$ means domain averaging). For 3D homogeneous isotropic turbulence, a constant $C_S = 0.17$ was analytically derived from the energy spectrum scaling (Lilly 1967; Pope 2001). Empirically, it was found that 0.17 leads to the best *a-priori* performance (McMillan & Ferziger 1979). For 2D turbulence, no analytical or empirical estimate exists for C_S or C_L , and trial and error is often used to select a value (Maulik *et al.* 2019). For both closures, C can be also determined dynamically (DSmag, DLeith) from the Germano identity (Germano *et al.* 1991; Grooms 2023). However, this procedure can lead to $\nu_e < 0$ (backscattering) and unstable LES. While capturing backscattering is desirable (see below), in practice, DSmag and DLeith are used with “positive clipping”, which enforces $\nu_e \geq 0$ and makes the closure more diffusive (thus less accurate) in favor of stability.

To capture backscattering, which can be important in many flows (Sagaut 2006), including oceanic and atmospheric circulations (Juricke *et al.* 2020; Grooms 2023), backscattering closures have been developed that, for example, inject a fraction of the dissipated energy back to the resolved scales. Here, we use the recently developed closure of Jansen & Held (2014) (JH, hereafter), which has been applied to oceanic and quasi-geostrophic turbulence (Jansen *et al.* 2015; Ross *et al.* 2023). The JH closure is

$$\Pi^{\text{SGS}} = \nabla^2(\nu_e \nabla^2 \bar{\omega}) + \nu_b \nabla^2 \bar{\omega}, \quad \nu_b = -C_B \langle \bar{\psi} \nabla^2(\nu_e \nabla^2 \bar{\omega}) \rangle / \langle \bar{\psi} \nabla^2 \bar{\omega} \rangle, \quad (2.3)$$

where the first term is biharmonic eddy-viscosity, and the second term represents backscattering with anti-diffusion. C_B determines how much of the globally dissipated energy is fed back into the resolved scales. ν_e can be determined in the same way as in Leith (Jansen & Held 2014) or Smag (Jansen *et al.* 2015; Ross *et al.* 2023). Like

C_S and C_L , C_B is an empirically determined parameter that is expected to be $\mathcal{O}(1)$ to balance the forward transferred and backscattered energy. Jansen & Held (2014) showed that in general, $C_B \geq 0.9$, and used 0.9.

Here, we focus on four closures: Smag, Leith, JH-Smag (JHS), and JH-Leith (JHL). We estimate, as described below, their one or two *constant* parameters C for each case. For JHS and JHL, we define ν_e in similar ways as in Smag/Leith (Jansen & Held 2014; Jansen *et al.* 2015; Ross *et al.* 2023) but choose the power of $C\Delta$ consistent with the dimension of the biharmonic: $\nu_e = (C_{\text{JHS}}\Delta)^4 \langle \bar{S}^2 \rangle^{1/2}$ (JHS) and $\nu_e = (C_{\text{JHL}}\Delta)^5 \langle (\nabla \bar{\omega})^2 \rangle^{1/2}$ (JHL); note that to be consistent with other implementations, unlike JH14, we use domain averaging in the calculation of ν_e^{JHL} . Here, like C_S and C_L , parameters C_{JHS} , C_{JHL} , and C_B are dimensionless.

2.2. Calibration, emulation and sampling (CES) for online learning

We estimate the optimal C parameter(s) of a closure by matching the turbulent kinetic energy (TKE) spectra ($\hat{E}(k)$) of the filtered DNS (FDNS) and of the LES with that closure (we have also explored matching enstrophy spectra $\hat{Z}(k) = k^2 \hat{E}(k)$; see Section 4). More specifically, we minimize the following loss function with respect to the C value(s):

$$\mathcal{L} = \sum_k \left\{ \ln(\hat{E}^{\text{FDNS}}(k)) - \ln(\hat{E}^{\text{LES}}(k)), \Gamma_{\text{FDNS}}^{-1} \left(\ln(\hat{E}^{\text{FDNS}}(k)) - \ln(\hat{E}^{\text{LES}}(k)) \right) \right\} \quad (2.4)$$

where $\{, \}$ is the Euclidean inner product, Γ_{FDNS} is the covariance matrix of $\ln(\hat{E}^{\text{FDNS}})$, and $k = (k_x^2 + k_y^2)^{1/2}$. To obtain the FDNS data and to construct the training and testing datasets, we apply a low-pass sharp-spectral filter with cut-off wavenumber $k_c = L/(2\Delta) = N_{\text{LES}}/2$ to each DNS snapshot. Therefore, for each case, the FDNS spectrum matches that of the DNS up to k_c (Fig. 1). $\hat{E}(k)$ in (2.4), the only information from DNS needed for training, is calculated by averaging the $\hat{E}(k)$ profiles over 100 de-correlated FDNS snapshots (See Supplementary Material for more details). The DNS length for this number of FDNS snapshots is within the ‘‘small data’’ regime for these cases and not enough for *offline* training of an accurate and stable NN-based closure (Guan *et al.* 2023). Note that because $\hat{E}(k)$ is rather invariant for flows in statistical equilibrium, we could have used an even shorter DNS from each case, as $\hat{E}(k)$ spectra averaged over just the first 5 DNS snapshots (i.e., a $20\times$ shorter DNS) are virtually indistinguishable from those calculated from all 100 snapshots (see Fig. 1).

Minimizing loss functions such as (2.4) requires performing LES during the optimization process. Derivative-free techniques such as EKI can be used with any solver, as the solver does not have to be differentiable. To quantify the uncertainty of the estimated C value(s), we employ the calibrate, emulate, and sample (CES) framework (Cleary *et al.* 2021). The framework is well-established and now available as a software (Dunbar *et al.* 2024). The full CES process applied in this work is depicted in Fig. 2.

3. Results

Table 1 shows the EKI-optimized constant parameters of Smag, Leith, JHS, and JHL for all 8 cases. The C_S^{EKI} is around 0.12 and the same for all cases (within the $\mathcal{O}(0.01)$ uncertainty, see Supplementary Material Table 1). This value is smaller than the analytical and empirical value of 0.17 often used based on previous work with 3D

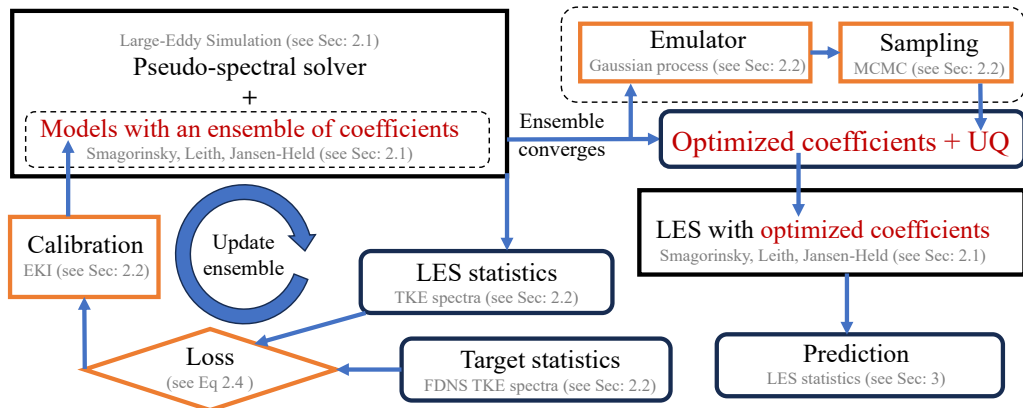


Figure 2: The schematic of the CES framework with EKI to estimate the closure parameters with uncertainty. Briefly, first, for a given case and closure, an ensemble of C values are generated by drawing 10 times from a Gaussian distribution (see Supplementary Material). For each C value(s), a long-enough LES is performed and the mean TKE spectrum of this ensemble member is computed. Then the loss is calculated against the target (FDNS spectrum) for each ensemble member. EKI is used to update the C values, and this process continues until the ensembles converge, which usually happens in 10 or fewer epochs (a typical convergence trend is shown in Supplementary Material Fig. 1). For uncertainty quantification (UQ), all parameters and their corresponding statistics from all epochs are used to train a Gaussian process emulator. This fast emulator is used for UQ with Markov-chain Monte Carlo (MCMC).

homogeneous isotropic turbulence. As shown below, the EKI-optimized value leads to significant improvements in *a-priori* and *a-posteriori* metrics over Smag with $C_S = 0.17$ (Smag-0.17). The C_L^{EKI} is around 0.24, and again, the same for all cases (within the estimated uncertainty). These values follow the relation $(C_S^{\text{EKI}})^2 \approx (C_L^{\text{EKI}})^3$, which is expected from dimensional analysis (Leith 1996). $C_{\text{JHS}}^{\text{EKI}}$ and $C_{\text{JHL}}^{\text{EKI}}$ are also found to be similar across all cases and around 0.215 and 0.295, respectively. They follow the expected relationship of $(C_{\text{JHS}}^{\text{EKI}})^4 \approx (C_{\text{JHL}}^{\text{EKI}})^5$. The backscattering parameter C_B^{EKI} is the same across all cases and around 0.95, which is between unity and the previously used value of 0.9. In summary, across these 8 cases, C_S , C_L , C_{JHS} , C_{JHL} and C_B in these 4 closures are found to be nearly constant.

For baselines in the *a-priori* and *a-posteriori* tests, we conduct LES with Π^{SGS} parameterized using Smag-0.17 and using DSmag and DLeith (with positive clipping) implemented following recent studies (Maulik & San 2016; Guan *et al.* 2023). LES with these 3 “baseline” closures and with the 4 EKI-optimized closures are conducted for each case. Each LES run is $100\times$ longer than the duration of the DNS used for the training dataset. As discussed below, for *a-priori* tests, we compare the total energy and enstrophy interscale transfers among these closures and FDNS. For *a-posteriori* tests, we compare the enstrophy spectra and vorticity PDFs from LES with different closures and from FDNS.

The global energy and enstrophy transfers are $\langle P_E \rangle = \langle \Pi^{\text{SGS}} \bar{\psi} \rangle$ and $\langle P_Z \rangle = \langle \Pi^{\text{SGS}} \bar{\omega} \rangle$, respectively (Thuburn *et al.* 2014; Guan *et al.* 2023). Here, $\langle P_E \rangle$ or $\langle P_Z \rangle$ is positive for forward transfer (energy/enstrophy moving to SGS from resolved scales) and negative for backscatter (moving to resolved scales from SGS). $\langle P_E \rangle$ and $\langle P_Z \rangle$ from FDNS and LES for representative cases (1.1, 1.4, 2, 3.3) are shown in Fig. 3 (values for all cases are reported in Supplementary Material Table 2). It can be observed that for all cases, JHS and JHL have the best agreement with FDNS, and

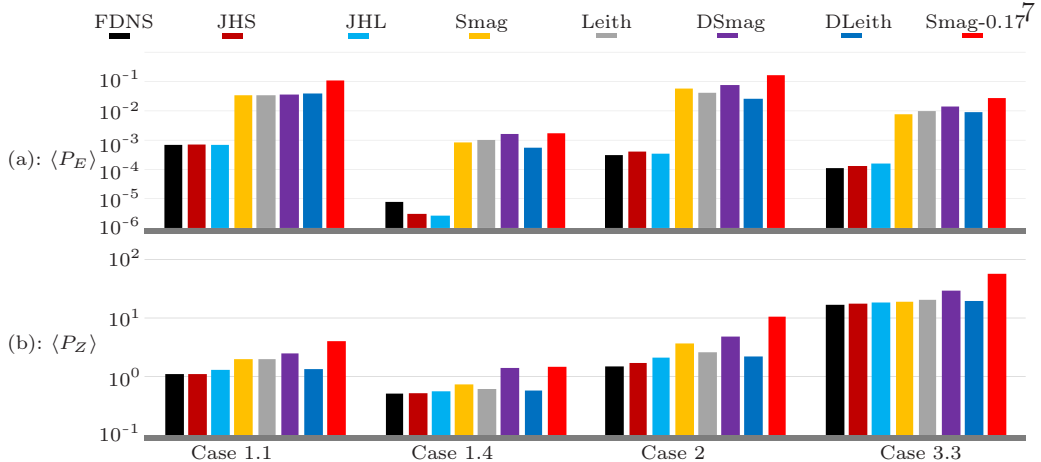


Figure 3: Interscale transfers in representative cases calculated *a-priori* for the same FDNS samples (note the logarithmic scale). EKI-optimized closures (JHS, JHL, Smag, and Leith) are compared against baselines (DSmag, DLeith, and Smag-0.17) and the truth (FDNS). Values for all 8 cases are shown in Supplementary Material Table 2.

for half of the cases, the values of $\langle P_E \rangle$ and $\langle P_Z \rangle$ closely match those of FDNS. Exceptions are Cases 1.2, 1.3, 1.4, and 3.1, for which JHS and JHL under-predict $\langle P_E \rangle$ by a factor of 2–3; however, they still significantly outperform the optimized Smag and Leith and the baselines, which over-predict $\langle P_E \rangle$ by 1 and even 2 orders of magnitude (thus, these closures are too diffusive). The gain from optimization can be isolated by comparing Smag and Smag-0.17: the former, which uses $C_S \approx 0.12$, consistently outperforms the baseline in both $\langle P_E \rangle$ and $\langle P_Z \rangle$ (often by a factor of 2 to 5, or even larger).

Next, we examine the enstrophy spectra, $\hat{Z}(k)$, and the PDF of vorticity, $\mathcal{P}(\omega)$. Figure 4 shows $\hat{Z}(k)$ for representative cases. Smag-0.17 and DSmag, consistent with $\langle P_Z \rangle$ in Fig. 3, have excessive enstrophy dissipation and under-predict, by about an order of magnitude, \hat{Z} compared to FDNS at the smallest scales. Among the baselines, DLeith performs the best in matching the FDNS, but it is still not comparable to EKI-optimized models. All the EKI-optimized closures work well in matching the FDNS \hat{Z} , which is not surprising given that their target was TKE spectra. The one exception is Case 3.3, where only optimized JH closures (and to a lesser degree Leith) can match the FDNS \hat{Z} in the largest scales (small k).

Figure 5 shows PDF $\mathcal{P}(\bar{\omega})$ for representative cases. Except for Cases 1.3 and 1.4 for which LES with all closures match the FDNS’ PDF well (down to the tails), for all other cases, LES with optimized JH closures clearly outperform the baselines and optimized Smag and Leith in matching the FDNS \mathcal{P} , especially at the tails (rare, extreme events). In fact, except for Case 1.1, which involves the largest $N_{\text{DNS}}/N_{\text{LES}} = 32$, LES with optimized JH matches the FDNS’ \mathcal{P} well. LES with optimized Smag and Leith also outperform the baselines (see, e.g., 3.3), although for Cases 1.1, 1.2, and 3.1, DLeith shows comparable performance.

4. Summary and Conclusion

We use the CES framework with EKI to learn *online* the constant parameters of four well-known physics-based models for 8 setups of 2D geophysical turbulence. The objective of the learning process is to match the TKE spectrum \hat{E} of LES with the

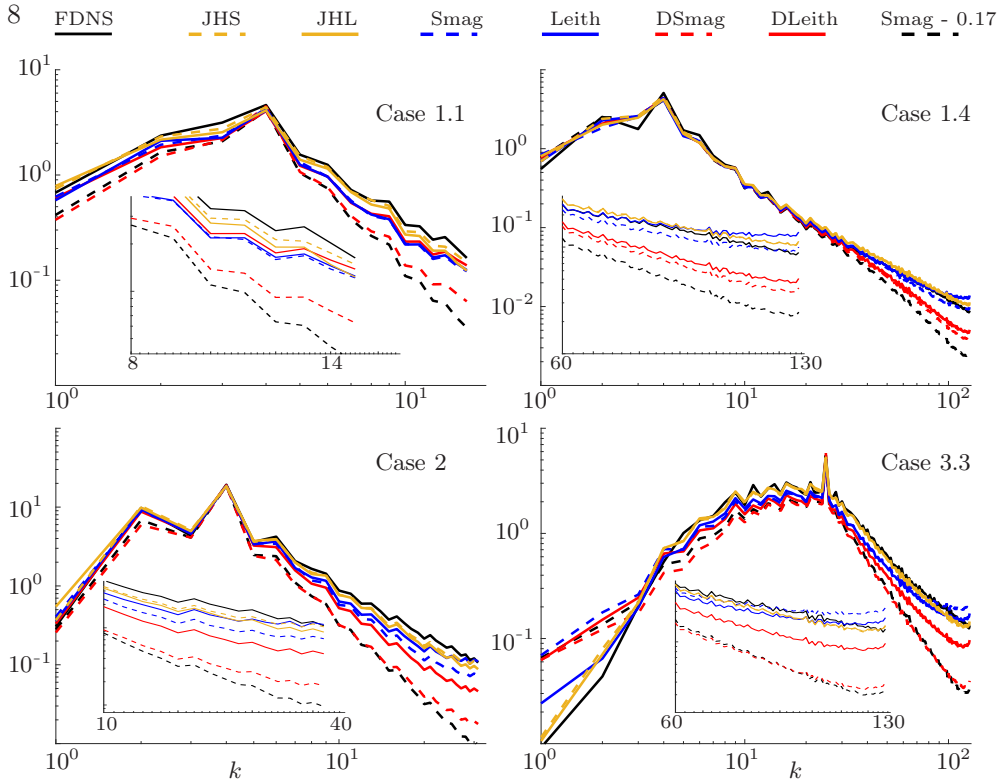


Figure 4: Enstrophy spectra (\hat{Z}) from FDNS and LES for representative cases (see Supplementary Material for other cases). The insets magnify the high- k part of spectra.

optimized closure with the spectrum of FDNS. The latter can be obtained from a short DNS run, making the approach *data-efficient*. Note that we have also explored using the enstrophy spectrum \hat{Z} of FDNS as the target for learning C_S and C_L for Case 3.1, and found similar constant parameters (1.2 vs. 1.3 and 2.4 vs. 2.4), which is not surprising given the simple relationship between \hat{Z} and \hat{E} . The estimated parameters of each closure are found to be nearly constant across the 8 cases, suggesting that the optimized closures are *generalizable*. In a follow-up study, we will aim to further investigate this universality of the constants through turbulence theory and scaling analysis. Such analysis will provide further insight into these already *interpretable* closures.

A number of metrics are used to quantify the performance of the optimized closures. The *a-priori* metrics involving mean interscale energy and enstrophy transfers (between the SGS and resolved flow) show major improvements resulting from optimization. In particular, the backscattering model (JH) demonstrates significantly better ability in capturing these transfers compared to baselines and optimized eddy-viscosity models. *A-posteriori* tests, focused on examining the enstrophy spectra at the largest and smallest length scales and the tails of the vorticity PDFs, again show major improvements gained from the optimization. Overall, the optimized eddy-viscosity closures are found to work well (and better than the baselines) except for cases in which the LES resolution is low compared to the forcing length scale (i.e., small k_c/k_f). For such cases, the eddy-viscosity closures have structural errors, and optimization alone (which only addresses parameteric errors) cannot further improve

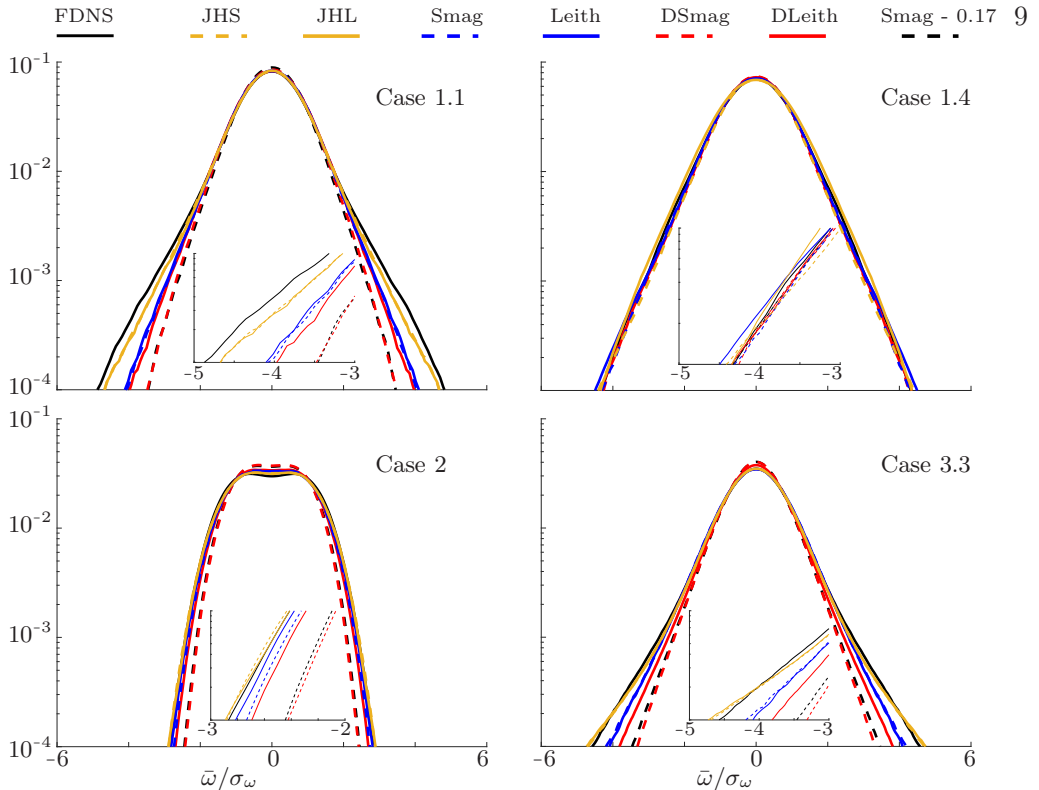


Figure 5: PDFs of $\bar{\omega}$ normalized by the standard deviation of FDNS (σ_ω) for representative cases (see Supplementary Material for other cases). The insets zoom into the left tails. Kernel estimator with a bandwidth of 1 is used to generate the PDFs.

the LES. The JH closure, on the other hand, leads to LES that matches FDNS closely based on all metrics and for all cases, further showing the importance of combining theoretical advances and data-driven techniques to develop data-efficient frameworks for accurate, interpretable, and generalizable closures. The next steps in this work should include exploring cases with more extreme regimes (e.g., higher Re) and different dynamics, and investigating more complex test cases (e.g., ocean general circulation models).

Acknowledgments

We thank Karan Jakhar, Malte Jansen, and Rambod Mojgani for insightful discussions. This work was supported by ONR award N000142012722, NSF grants OAC-2005123 and AGS-1835860, and by Schmidt Sciences, LLC. Computational resources were provided by ACCESS (ATM170020) and CISL (URIC0004). Codes/data are available at <https://github.com/envfluids/2D-DDP> and <https://clima.github.io/CalibrateEmulateSample.jl/>.

REFERENCES

- BECK, A., FLAD, D. & MUNZ, C.-D. 2019 Deep neural networks for data-driven LES closure models. *Journal of Computational Physics* **398**, 108910.
 BEUCLER, T., GENTINE, P., YUVAL, J., GUPTA, A., PENG, L., LIN, J., YU, S., RASP, S.,

- AHMED, F., O'GORMAN, P. A. & OTHERS 2024 Climate-invariant machine learning. *Science Advances* **10** (6), eadj7250.
- BRACCO, A., BRAJARD, J., DIJKSTRA, H. A., HASSANZADEH, P., LESSIG, C. & MONTELEONI, C. 2024 Machine learning for the physics of climate. *arXiv:2408.09627* .
- CLEARY, E., GARBUNO-INIGO, A., LAN, S., SCHNEIDER, T. & STUART, A. M. 2021 Calibrate, emulate, sample. *Journal of Computational Physics* **424**, 109716.
- DUNBAR, O. R., BIELI, M., GARBUNO-INIGO, A., HOWLAND, M., DE SOUZA, A. N., MANSFIELD, L. A., WAGNER, G. L., EFRAT-HENRICI, N. & OTHERS 2024 Calibrateemulatesample. jl: Accelerated parametric uncertainty quantification. *Journal of Open Source Software* **9** (97), 6372.
- EYRING, V., COLLINS, W. D., GENTINE, P., BARNES, E. A., BARREIRO, M., BEUCLER, T., BOCQUET, M., BRETHERTON, C. S., CHRISTENSEN, H. M., DAGON, K. & OTHERS 2024 Pushing the frontiers in climate modelling and analysis with machine learning. *Climate Change* pp. 1–13.
- FREZAT, H., LE SOMMER, J., FABLET, R., BALARAC, G. & LGUENSAT, R. 2022 A posteriori learning for quasi-geostrophic turbulence parametrization. *Journal of Advances in Modeling Earth Systems* **14** (11).
- GERMANO, M., PIOMELLI, U., MOIN, P. & CABOT, W. H. 1991 A dynamic subgrid-scale eddy viscosity model. *Physics of Fluids A: Fluid Dynamics* **3** (7), 1760–1765.
- GROOMS, I. 2023 Backscatter in energetically-constrained leith parameterizations. *Ocean Modelling* **186**.
- GUAN, Y., CHATTOPADHYAY, A., SUBEL, A. & HASSANZADEH, P. 2022 Stable a posteriori LES of 2D turbulence using convolutional neural networks: Backscattering analysis and generalization to higher Re via transfer learning. *Journal of Computational Physics* **458**, 111090.
- GUAN, Y., SUBEL, A., CHATTOPADHYAY, A. & HASSANZADEH, P. 2023 Learning physics-constrained subgrid-scale closures in the small-data regime for stable and accurate les. *Physica D* **443**, 133568.
- JAKHAR, K., GUAN, Y., MOJGANI, R., CHATTOPADHYAY, A. & HASSANZADEH, P. 2024 Learning closed-form equations for subgrid-scale closures from high-fidelity data: Promises and challenges. *Journal of Advances in Modeling Earth Systems* **16** (7), e2023MS003874.
- JANSEN, M. F. & HELD, I. M. 2014 Parameterizing subgrid-scale eddy effects using energetically consistent backscatter. *Ocean Modelling* **80**, 36–48.
- JANSEN, M. F., HELD, I. M., ADCROFT, A. & HALBERG, R. 2015 Energy budget-based backscatter in an eddy permitting primitive equation model. *Ocean Modelling* **94**, 15–26.
- JURICKE, S., DANILOV, S., KOLDUNOV, N., OLIVER, M., SEIN, D., SIDORENKO, D. & WANG, Q. 2020 A kinematic kinetic energy backscatter parametrization: From implementation to global ocean simulations. *Journal of Advances in Modeling Earth Systems* **12** (12), e2020MS002175.
- KENNEDY, M. C. & O'HAGAN, A. 2002 Bayesian Calibration of Computer Models. *Journal of the Royal Statistical Society Series B: Statistical Methodology* **63** (3), 425–464.
- LAI, C.-Y., HASSANZADEH, P., SHESHADRI, A., SONNEWALD, M., FERRARI, R. & BALAJI, V. 2024 Machine learning for climate physics and simulations. *arXiv:2404.13227* .
- LEITH, C. 1996 Stochastic models of chaotic systems. *Physica D* **98** (2-4), 481–491.
- LILLY, D. K. 1967 The representation of small-scale turbulence in numerical simulation experiments. In *Proc. IBM Sci. Comput. Symp. on Environmental Science*, pp. 195–210.
- LIST, B., CHEN, L.-W. & THUERNEY, N. 2022 Learned turbulence modelling with differentiable fluid solvers: physics-based loss functions and optimisation horizons. *Journal of Fluid Mechanics* **949**, A25.
- LOPEZ-GOMEZ, I., CHRISTOPOULOS, C., LANGELAND ERVIK, H. L., DUNBAR, O. R., COHEN, Y. & SCHNEIDER, T. 2022 Training physics-based machine-learning parameterizations with gradient-free ensemble kalman methods. *Journal of Advances in Modeling Earth Systems* **14** (8), e2022MS003105.
- MARTINEZ, V. R., MURRI, J. & WHITEHEAD, J. P. 2024 Relaxation-based schemes for on-the-fly parameter estimation in dissipative dynamical systems. *arXiv:2408.14296* .
- MAULIK, R. & SAN, O. 2016 Dynamic modeling of the horizontal eddy viscosity coefficient for

- quasigeostrophic ocean circulation problems. *Journal of Ocean Engineering and Science* **1**, 300–324.
- MAULIK, R., SAN, O., RASHEED, A. & VEDULA, P. 2019 Subgrid modelling for two-dimensional turbulence using neural networks. *Journal of Fluid Mechanics* **858**, 122–144.
- McMILLAN, O. J. & FERZIGER, J. H. 1979 Direct testing of subgrid-scale models. *AIAA Journal* **17** (12).
- MOJGANI, R., WAELCHLI, D., GUAN, Y., KOUMOUTSAKOS, P. & HASSANZADEH, P. 2023 Extreme event prediction with multi-agent reinforcement learning-based parametrization of atmospheric and oceanic turbulence. *arXiv:2312.00907* .
- NOVATI, G., DE LAROUSSILHE, H. L. & KOUMOUTSAKOS, P. 2021 Automating turbulence modelling by multi-agent reinforcement learning. *Nature Machine Intelligence* **3** (1), 87–96.
- PAHLAVAN, H. A., HASSANZADEH, P. & ALEXANDER, M. J. 2024 Explainable offline-online training of neural networks for parameterizations: A 1D gravity wave-QBO testbed in the small-data regime. *Geophysical Research Letters* **51** (2), e2023GL106324.
- POPE, S. B. 2001 *Turbulent Flows*. IOP Publishing.
- RASP, S., PRITCHARD, M. S. & GENTINE, P. 2018 Deep learning to represent subgrid processes in climate models. *Proceedings of the National Academy of Sciences* **115** (39), 9684–9689.
- ROSS, A., LI, Z., PEREZHOGIN, P., FERNANDEZ-GRANDA, C. & ZANNA, L. 2023 Benchmarking of machine learning ocean subgrid parameterizations in an idealized model. *Journal of Advances in Modeling Earth Systems* **15** (1), e2022MS003258.
- SAGAUT, P. 2006 *Large eddy simulation for incompressible flows*. Springer Science & Business Media.
- SANDERSE, B., STINIS, P., MAULIK, R. & AHMED, S. E. 2024 Scientific machine learning for closure models in multiscale problems: A review. *arXiv:2403.02913* .
- SCHNEIDER, T., BEHERA, S., BOCCALETTI, G., DESER, C., EMANUEL, K., FERRARI, R., LEUNG, L. R., LIN, N., MÜLLER, T., NAVARRA, A. & OTHERS 2023 Harnessing AI and computing to advance climate modelling and prediction. *Nature Climate Change* **13** (9), 887–889.
- SCHNEIDER, T., JEEVANJEE, N. & SOCOLOW, R. 2021 Accelerating progress in climate science. *Physics Today* **74** (6), 44–51.
- SCHNEIDER, T., LEUNG, L. R. & WILLS, R. C. 2024 Opinion: Optimizing climate models with process-knowledge, resolution, and AI. *EGU sphere* **2024**, 1–26.
- SHANKAR, V., MAULIK, R. & VISWANATHAN, V. 2023 Differentiable turbulence ii. *arXiv:2307.13533* .
- SIRIGNANO, J., MACART, J. F. & FREUND, J. B. 2020 DPM: A deep learning PDE augmentation method with application to large-eddy simulation. *Journal of Computational Physics* **423**, 109811.
- SMAGORINSKY, J. 1963 General circulation experiments with the primitive equations: I. The basic experiment. *Monthly Weather Review* **91** (3), 99–164.
- SRINIVASAN, K., CHEKROUN, M. D. & MCWILLIAMS, J. C. 2024 Turbulence closure with small, local neural networks: Forced two-dimensional and β -plane flows. *Journal of Advances in Modeling Earth Systems* **16** (4), e2023MS003795.
- SUBEL, A., GUAN, Y., CHATTOPADHYAY, A. & HASSANZADEH, P. 2023 Explaining the physics of transfer learning in data-driven turbulence modeling. *PNAS nexus* **2** (3), pgad015.
- SUN, Y. Q., HASSANZADEH, P., ALEXANDER, M. J. & KRUSE, C. G. 2023 Quantifying 3D gravity wave drag in a library of tropical convection-permitting simulations for data-driven parameterizations. *Journal of Advances in Modeling Earth Systems* **15** (5), e2022MS003585.
- THUBURN, J., KENT, J. & WOOD, N. 2014 Cascades, backscatter and conservation in numerical models of two-dimensional turbulence. *Quarterly Journal of the Royal Meteorological Society* **140**, 626–638.
- WU, J.-L., LEVINE, M. E., SCHNEIDER, T. & STUART, A. 2024 Learning about structural errors in models of complex dynamical systems. *Journal of Computational Physics* p. 113157.
- YUVAL, J. & O’GORMAN, P. A. 2023 Neural-network parameterization of subgrid momentum

- transport in the atmosphere. *Journal of Advances in Modeling Earth Systems* **15** (4), e2023MS003606.
- ZANNA, L. & BOLTON, T. 2020 Data-driven equation discovery of ocean mesoscale closures. *Geophysical Research Letters* **47** (17), e2020GL088376.
- ZHANG, X.-L., XIAO, H., LUO, X. & HE, G. 2022 Ensemble kalman method for learning turbulence models from indirect observation data. *Journal of Fluid Mechanics* **949**, A26.